

THE RESOLVED NEAR-INFRARED EXTRAGALACTIC BACKGROUND

R. C. KEENAN¹, A. J. BARGER^{1,2,3}, L. L. COWIE³, W.-H. WANG⁴*Draft version August 26, 2010*

ABSTRACT

We present a current best estimate of the integrated near-infrared (NIR) extragalactic background light (EBL) attributable to resolved galaxies in J , H , and K_s . Our results for measurements of $\nu I \nu$ in units of $\text{nW m}^{-2} \text{sr}^{-1}$ are $11.7^{+5.6}_{-2.6}$ in J , $11.5^{+4.5}_{-1.5}$ in H and $10.0^{+2.8}_{-0.8}$ in K_s . We derive these new limits by combining our deep wide-field NIR photometry from five widely separated fields with other studies from the literature to create a galaxy counts sample that is highly complete and has good counting statistics out to $JHK_s \sim 27-28$. As part of this effort we present new ultra-deep K_s -band galaxy counts from 22 hours of observations with the Multi Object Infrared Camera and Spectrograph (MOIRCS) instrument on the Subaru Telescope. We use this MOIRCS K_s -band mosaic to estimate the total missing flux from sources beyond our detection limits. Our new limits to the NIR EBL are in basic agreement with, but 10–20% higher than previous estimates, bringing them into better agreement with estimates of the total NIR EBL (resolved + unresolved sources) obtained from TeV γ -ray opacity measurements and recent direct measurements of the total NIR EBL. We examine field to field variations in our photometry to show that the integrated light from galaxies is isotropic to within uncertainties, consistent with the expected large-scale isotropy of the EBL. Our data also allow for a robust estimate of the NIR light from Galactic stars, which we find to be 14.7 ± 2.4 in J , 10.1 ± 1.9 in H and 7.6 ± 1.8 in K_s in units of $\text{nW m}^{-2} \text{sr}^{-1}$.

Subject headings: cosmology: observations — galaxies: fundamental parameters (counts, near-infrared background)

1. INTRODUCTION

The near-infrared (NIR) extragalactic background light (EBL) is the total light from resolved and unresolved extragalactic sources in the NIR. This represents the integrated light from all star and galaxy formation processes over the history of the universe that has been redshifted into the NIR. Some fraction of the NIR EBL can be resolved as the light from individual galaxies (Integrated Galaxy Light, IGL), but the fractional contribution from unresolved (and perhaps unresolvable) sources is not well constrained. A measurement of the total NIR EBL minus the IGL will provide insight into the energy budget of the early universe.

While direct unresolved measurement of the NIR EBL is technically difficult due to complex foregrounds, several authors have reported a measurement of the total (resolved plus unresolved) NIR EBL (Hauser et al. 1998; Dwek & Arendt 1998; Gorjian et al. 2000; Wright 2001; Matsumoto 2001; Matsumoto et al. 2005; Cambr sy et al. 2001; Levenson et al. 2007) and found it to be a factor of two or more above the IGL obtained through source counts (Madau & Pozzetti 2000; Totani et al. 2001; Thompson 2003). This is known as the NIR background excess (NIRBE). The spectral energy distribution (SED) of this measured excess, in some cases, appears very similar to that of zodiacal light, which suggests there may be a foreground contamination is-

sue. Another possible solution to this excess is a large population of undetected faint galaxies and/or population III (PopIII) stars contributing a large fraction of the NIR background (see Kashlinsky 2005; Hauser & Dwek 2001 for reviews). For example, Matsumoto et al. (2005) found a large NIRBE with a distinct spectral break at $\sim 1\mu\text{m}$, which they interpreted as a possible signature of a Lyman limit break in PopIII stellar spectra at a redshift of ~ 10 .

Since the NIR EBL presents a source of opacity for TeV γ -rays via pair production, the density of the background light can, in principle, be measured via direct observation of TeV blazars. This method relies on assumptions of the intrinsic blazar spectrum and the SED of the EBL from ultraviolet to the NIR, both of which are poorly observationally constrained. Nevertheless, TeV γ -rays provide an independent estimate of the NIR EBL that can be used to help determine what fraction of the background light can be attributed to resolved sources, and how much may arise from faint and possibly exotic sources in the early universe.

Dwek et al. (2005) explored the possibility that the NIRBE is of extragalactic origin by looking for the absorption imprint of the $\sim 1\mu\text{m}$ spectral break on the γ -ray SEDs of several TeV blazars. They concluded that the apparent NIR excess is likely not of extragalactic origin because its signature is not detected in the blazar SEDs. Recent observations of TeV blazars with the High Energy Stereoscopic System (HESS) have placed limits on the NIR EBL that allow for the possibility of little or no excess above integrated galaxy counts (Aharonian et al. 2006).

Mazin & Raue (2007) used 13 TeV blazars and a grid of NIR background SEDs to further constrain the back-

¹ Department of Astronomy, University of Wisconsin-Madison, 475 N. Charter Street, Madison, WI 53706

² Department of Physics and Astronomy, University of Hawaii, 2505 Correa Road, Honolulu, HI 96822

³ Institute for Astronomy, University of Hawaii, 2680 Woodlawn Drive, Honolulu, HI 96822

⁴ Institute of Astronomy and Astrophysics, Academia Sinica, P.O. Box 23-141, Taipei 10617, Taiwan.

ground light. They derived limits on the NIR EBL that are roughly in agreement with those of Aharonian et al. (2006). However, systematic uncertainties in these γ -ray opacity measurements due to uncertainties in the blazar SED and that of the EBL result in large error bars that could still allow for a significant NIRBE (of the same order as the IGL) to be present, even if their assumptions about the intrinsic blazar SED and that of the EBL are assumed to be reasonable.

As such, the goal of this paper is to derive a firm lower limit to the NIR IGL so as to facilitate a robust comparison with future new results from direct and indirect measurements of the NIR EBL. We present the best current estimate of the NIR IGL by combining our deep wide-field NIR data set with a compilation of galaxy counts from the literature and ultra-deep K_s -band galaxy counts from a subfield of the Subaru MOIRCS image presented in Barger et al. (2008) and Wang et al. (2009).

The structure of this paper is as follows: We describe our NIR dataset briefly in Section 2. We calculate the contribution of resolved galaxies to the NIR EBL in Section 3. We compare with previous measurements of the NIR EBL and IGL and discuss the implications of our results in Section 4. We summarize in Section 5. Unless otherwise noted, all magnitudes given in this paper are in the AB magnitude system ($m_{AB} = -2.5 \log f_\nu - 48.60$ with f_ν in units of $\text{ergs cm}^{-2} \text{s}^{-1} \text{Hz}^{-1}$).

2. THE NIR DATA

We presented the observations, data reduction, star-galaxy separation, and bright galaxy counts for our deep wide-field NIR dataset in Keenan et al. (2010) (K10 hereafter). The data consist of five widely separated fields at high galactic latitudes, including one centered on an Abell cluster (Abell 370). The survey covers approximately 3 deg^2 reaching a 5σ limiting magnitude of $JHK_s \sim 22 - 23$ over $\sim 2.75 \text{ deg}^2$ with another $\sim 0.25 \text{ deg}^2$ to $JHK_s \sim 24$, making it one of the deepest wide-field surveys to date in the NIR. The fields covered in this survey are described in Section 2.1.

In this paper we supplement the above data with those from an ultra-deep K_s -band mosaic composed of imaging done by our group and Japanese groups led by various investigators using the Multi Object InfraRed Camera and Spectrograph (MOIRCS) instrument on the 8.2 m Subaru Telescope. The MOIRCS imaging is described in Section 2.2.

2.1. Wide-Field Imaging and Galaxy Counts

Our first two fields are centered on the *Chandra* Large Area Synoptic X-ray Survey (CLASXS; Yang et al. 2004; Steffen et al. 2004) and the *Chandra* Lockman Area North Survey (CLANS; Trouille et al. 2008, 2009). Each of these fields cover $\sim 1 \text{ deg}^2$ in JHK_s . These fields are located in the Lockman Hole region of extremely low Galactic HI column density (Lockman et al. 1986). Our third field covers a 0.25 deg^2 area centered on the *Chandra* Deep Field North (CDF-N, Brandt et al. 2001; Alexander et al. 2003). The CDF-N contains the Great Observatories Origins Deep Survey North (GOODS-N; 145 arcmin^2 *HST* Advanced Camera for Surveys observation, Giavalisco et al. 2004). Our fourth field is the

Abell 370 (A370) cluster and surrounding area ($\sim 0.5 \text{ deg}^2$). A370 is a cluster of richness 0 at a redshift of $z = 0.37$. Our fifth field is a $\sim 0.2 \text{ deg}^2$ area centered on the “Small-Survey-Area 13” (SSA13) from the Hawaii Deep Fields described in Lilly et al. (1991).

In K10 we used the bright NIR galaxy counts from our survey in combination with counts we generated from The Two Micron All Sky Survey (2MASS, Skrutskie et al. 2006), The UKIRT Infrared Deep Sky Survey (UKIDSS, Lawrence et al. 2007) and other selections from the literature to explore local large scale structure via the slope of the galaxy counts curve as a function of position on the sky. Here we extend the counts from K10 to fainter magnitudes using the methods described below.

We generated average galaxy counts for our ensemble of NIR images by the methods described in K10. We corrected the counts for completeness through a simulation in which relatively bright ($JHK_s = 19$) galaxies were extracted from each image and then scattered at random to other parts of the image to test how well they were recovered as a function of apparent magnitude. We faded the test galaxies in 0.25 magnitude steps until the recovered fraction fell below 25%. We only included counts in the final average where completeness was better than 50%.

In our completeness simulations, given that we know the total magnitude of objects we are scattering throughout the image, we are able to compare the recovered magnitudes in various apertures to total magnitudes and thereby derive a magnitude correction factor for faint objects. Figure 1 shows example results from this exercise. In Figure 1a we show the fractional completeness ($N_{\text{recovered}}/N_{\text{scattered}}$) as a function of apparent magnitude for the CDF-N K_s -band. In all fields we reliably recover, on average, relatively bright objects ($JHK_s < 20$) at the correct magnitude using the SExtractor MAG_AUTO, which fits a Kron-like elliptical aperture to each object (Kron 1980). We find that the $3''$ aperture shows a roughly constant offset (~ -0.2) from total magnitude. Based on these results, we measure total magnitudes in the MAG_AUTO aperture for objects brighter than 20^{th} magnitude and switch to corrected 3 arcsecond aperture magnitudes for objects fainter than 20^{th} magnitude using the measured difference at 20^{th} magnitude. This magnitude correction only affects our calculated IGL at the $0.1 \text{ nW m}^{-2} \text{sr}^{-1}$ level, which is roughly a factor of 10 below the uncertainty in the IGL due to the uncertainty in the counts themselves.

2.2. MOIRCS Imaging and Galaxy Counts

The Subaru MOIRCS K_s -band image is centered on the GOODS-N field (Giavalisco et al. 2004). Part of the Japanese data were published in Kajisawa et al. (2006). Here we include all data taken between 2005 and 2008. The data reduction for the MOIRCS mosaic is described in Barger et al. (2008) and Wang et al. (2009) and is essentially the same as that used in K10.

K_s -band galaxy counts from the MOIRCS mosaic presented here are taken from a subfield of $\sim 15 \text{ arcmin}^2$ with an integration time of $\sim 22 \text{ hr}$ yielding a 5σ limit of ~ 26.5 . This MOIRCS image is, therefore, approximately as deep as the Subaru Deep Field

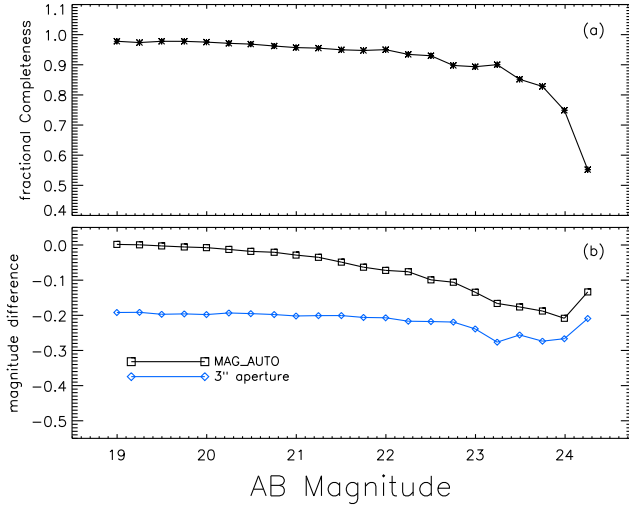


FIG. 1.— Example results from our completeness simulations (this case is for the CDF-N K_s -band, though results are similar across all fields). (a) Fractional completeness as a function of apparent magnitude. Asterisks and solid black line show fractional completeness ($N_{\text{recovered}}/N_{\text{scattered}}$) as a function of apparent magnitude (b) Magnitude difference as a function of apparent magnitude comparing the MAG_AUTO and 3'' apertures and showing total magnitude minus recovered magnitude for the two different apertures. Black squares show results for the MAG_AUTO aperture and blue diamonds for a 3'' aperture. The MAG_AUTO aperture does a good job at recovering total magnitude for objects brighter than 20th magnitude, and the 3'' aperture shows a roughly constant offset (~ -0.2) from total magnitude.

(SDF, Maihara et al. 2001) and Subaru Super Deep Field (SSDF, Minowa et al. 2005) but more than an order of magnitude larger in area on the sky than either survey.

We generated a catalog for the MOIRCS field using SExtractor software version 2.4.4 (Bertin & Arnouts 1996) for source identification and photometry. We used the MAG_AUTO aperture and set the minimum number of contiguous pixels to be considered a detection (SExtractor parameter DETECT_MINAREA) to 2 in order to push the counts on the faint end. We did not remove stars from the MOIRCS counts because we begin counting galaxies at 23rd magnitude where stars identifiable through color selection do not contribute significantly to galaxy counts ($\sim 1\%$ for $JHK_s = 23$ from K10 star counts compared with average galaxy counts from this paper). Cool dwarf stars unidentifiable through color selection may contaminate the counts on a slightly higher level, but their space density is unknown and we have no means of separating them from galaxies.

For the Subaru MOIRCS K_s -band data, we do not correct for completeness or total magnitudes. Rather, we calculate the total missing flux in the image using a method similar to that employed by Thompson et al. (2007). We discuss this in more detail in Section 3.1. We adopted this method because it allows us to not only account for the flux in objects missed near our detection limit (completeness correction), but also for the flux missed in objects or parts of objects below our detection limit. In J -band and H -band we adopt the missing flux estimates of Thompson et al. (2007).

3. NIR BACKGROUND DUE TO RESOLVED GALAXIES

In Figure 2 we show our completeness-corrected and averaged galaxy counts with those drawn from the literature. However, before combining all of our data in this way, we first investigated field to field variations for the IGL for our five fields over the magnitude range $14.5 < JHK_s < 22.5$ where all five are highly complete and have good counting statistics. We found the IGL over this magnitude range to be consistent across the four non-cluster fields (CLASXS, CLANS, CDF-N and SSA13 $\sim 7 - 8 \text{ nW m}^{-2} \text{ sr}^{-1}$) with a 1σ dispersion of $\pm 0.5 \text{ nW m}^{-2} \text{ sr}^{-1}$. As such, we find that the IGL is consistent with large-scale isotropy, an expected signature of the EBL (see Kashlinsky 2005; Hauser & Dwek 2001 for reviews).

In the A370 cluster field, our IGL measurements were $\sim 2 - 3 \text{ nW m}^{-2} \text{ sr}^{-1}$ higher in all bands with the peak contribution to the excess light arising from galaxies at $JHK_s \sim 17$, consistent with an excess of L_* galaxies at a redshift of ~ 0.4 as in A370. We include the cluster field in our average counts for this study because in a survey of a few square degrees such as this, roughly one massive cluster will be present.

In Figure 2 we use black diamonds to denote the counts for our five wide fields and black squares to denote counts for the MOIRCS image. The counts determined by K10 from the 2MASS field with Galactic latitudes of $|b| > 30$ are denoted by red asterisks. The counts determined by K10 from the 2MASS-6x Lockman Hole survey are denoted by green triangles. The counts determined by K10 from three subfields of the UKIDSS LAS are denoted by blue plus symbols. The three subfields that make up this section of the LAS are described in detail in K10. Other data points are taken from the publications listed in the plots. The dashed curves represent the error-weighted least squares running average from which we calculate the IGL. We describe the methods we used to calculate this average in Section 3.

Figures 2(d-f) display the same data as in panels (a-c) after dividing by an arbitrarily normalized Euclidean model (of $\alpha = 0.4$ in the form $N(m) = A \times 10^{\alpha m}$, and A is a constant) to expand the ordinate and demonstrate where resolved galaxies contribute the most to the IGL. A flat line in (d-f) would imply an equal contribution to the IGL at all magnitudes. The areas of positive slope show where galaxies contribute a larger fraction to the IGL as one moves toward fainter magnitude. The steep negative slope beyond $JHK_s > 23 - 24$ demonstrates the diminishing contribution of resolved galaxies to the IGL at the faintest magnitudes.

To calculate the IGL from all the counts data displayed in Figure 2, we used an error-weighted least-squares fit of the the slope and normalization parameters “A” and “ α ” in the function $N(m) = A \times 10^{\alpha m}$. We fit the data over a range of ± 2 magnitudes above and below each magnitude bin to get two estimates for the counts in that bin. In other words, at a given apparent magnitude “ m ”, we fit the range $m - 2$ to m and m to $m + 2$ separately. Each fit yielded an estimate of the counts at apparent magnitude m . We then recorded the average of these two values as the best estimate for counts in that bin. Each of the two fits also yielded a 1σ confidence interval for the counts in each bin. Given these fitted values and

TABLE 1
AVERAGE GALAXY COUNTS USED TO CALCULATE THE NIR EBL

J			H		K_s	
Mag(AB) ^a	Log ₁₀ (N) ^b	Log ₁₀ (ΔN) ^c	Log ₁₀ (N)	Log ₁₀ (ΔN)	Log ₁₀ (N)	Log ₁₀ (ΔN)
11	-1.31	-2.33	-1.13	-2.67	-1.27	-2.76
12	-0.67	-2.10	-0.51	-2.02	-0.63	-1.94
13	-0.06	-1.27	0.089	-1.60	-0.01	-1.64
14	0.500	-1.30	0.660	-0.25	0.603	-0.92
15	1.084	0.121	1.262	-0.32	1.229	0.553
16	1.654	0.726	1.842	1.004	1.891	0.379
17	2.290	1.517	2.425	1.519	2.592	2.013
18	2.910	2.365	3.030	1.786	3.149	1.851
19	3.340	2.665	3.453	2.644	3.554	2.228
20	3.713	3.117	3.825	2.736	3.901	2.479
21	4.098	3.495	4.148	3.368	4.200	2.701
22	4.455	3.811	4.488	3.476	4.459	2.946
23	4.719	4.162	4.781	4.059	4.795	3.669
24	4.916	4.391	4.965	4.170	5.008	3.931
25	5.067	4.242	5.156	4.732	5.178	4.653
26	5.285	4.439	5.297	4.647	5.324	4.618
27	5.370	4.297	5.361	5.055	5.462	5.227
28	5.376	4.717	5.456	4.755	5.547	4.983

^a AB Magnitude.

^b *N* is the surface density of galaxies in units of mag⁻¹deg⁻².

^c ΔN is the 1 σ error estimate for *N* (in the same units) derived from the fits described in Section 3 to all the data shown in Figure 2.

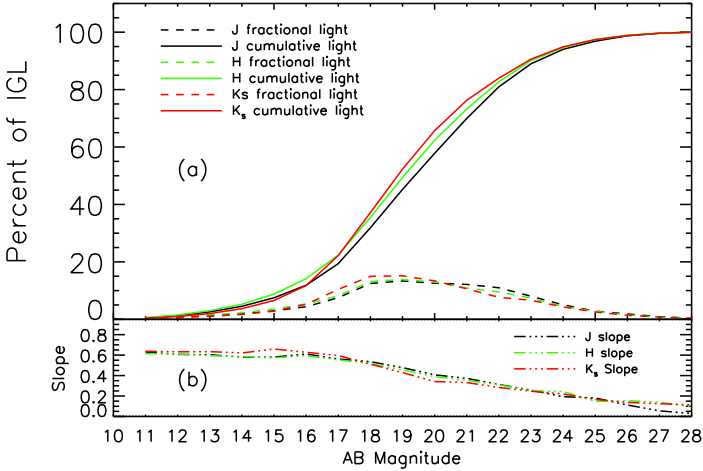


FIG. 3.— (a) Percent contribution to the IGL as a function of apparent magnitude. Solid curves show the cumulative contribution from galaxies to the NIR IGL as a function of apparent magnitude. Dashed curves show the fractional contribution per each magnitude bin. This demonstrates that the vast majority of the IGL ($\sim 90\%$) arises from galaxies in the apparent magnitude range $\sim 15 < JHK_s < 24$ where this study is highly complete and has good counting statistics. (b) Slope of the galaxy counts curve as a function of apparent magnitude. Dash-dotted curves show the measured slope of the galaxy counts curve as a function of apparent magnitude. When the slope drops below $\alpha = 0.4$ the total light from galaxies becomes convergent.

to be so numerous as to be unresolvable. As such, it may be safe to say that the resolvable portion of the NIR EBL (the IGL) has, for the most part, been measured and that the most important contribution to the resolved portion comes from galaxies in the magnitude range $\sim 15 < JHK_s < 24$, for which the deep wide-field data presented here are optimized.

3.1. *K_s*–band Faint Counts Slope and Missing Flux

We use our ultra-deep MOIRCS data to test for a possible steepening of the counts slope at faint magnitudes in the *K_s*–band, as appeared possible from the SDF (Maihara et al. 2001) and SSDF (Minowa et al. 2005) *K_s*–band counts. We see from Figure 2c, that the slope of the counts in the MOIRCS field continues to become flatter out to the faintest magnitudes. We detect no up-turn in the slope for very faint galaxies. As mentioned above, the MOIRCS counts have not had a completeness correction applied. Such a correction would steepen the curve slightly at the faintest magnitudes, but this effect would not be strong enough to alter significantly the trend in slope.

Thompson et al. (2007) estimated the missing flux component in the *J* and *H*–bands from the faint outer parts of galaxies and from galaxies below their detection limits using a histogram of flux in all pixels associated with detected objects. We use a similar method to estimate the flux missed in the *K_s*–band. In Figure 4 we show a histogram of number of pixels versus flux for all pixels associated with detected galaxies (object pixels) in our MOIRCS *K_s*–band mosaic. Noting the linear trend for fluxes $\sim 0.005 - 0.4 \mu\text{Jy}$, we fit a line to the data over this range (blue dashed line). The portion of the histogram used in the fit represents 60% of all object pixels in the image and 99% of object pixels with fluxes greater than the turnover in the histogram at $\sim 0.005 \mu\text{Jy}$. The slope of the linear fit is -0.86 . Thompson et al. (2007) find a slightly steeper value of -1 by simply estimating the slope by eye. Assuming that the true flux distribution for faint pixels ($< 0.005 \mu\text{Jy}$) continues along the same trend, we extrapolate the linear fit to approximate the shape of the histogram when all pixels in the image are accounted for. Using this method, we calculate an estimate for flux missed in the faint outer parts of galaxies and in galaxies that are below our detection limits. We find the missing flux component to be $\sim 22\%$ ($1.9 \text{ nW m}^{-2} \text{ sr}^{-1}$) of the total *K_s*–band light from resolved

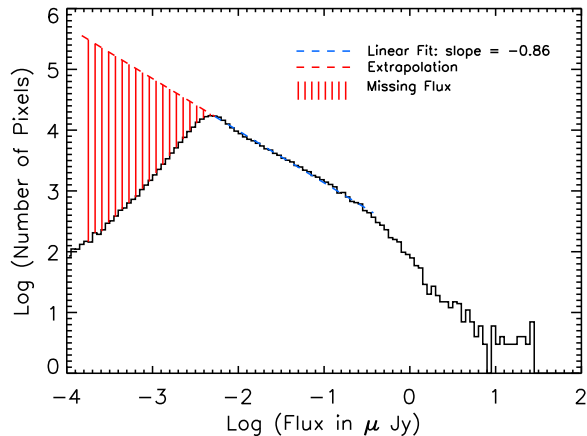


FIG. 4.— Histogram showing Log_{10} of flux in μJy vs. Log_{10} of the number of pixels at that flux for all the pixels associated with galaxies in the Subaru MOIRCS K_s -band image. The blue dashed line shows a linear fit from ~ 0.005 – $0.4 \mu\text{Jy}$, which includes $\sim 60\%$ of all pixels associated with galaxies and $\sim 99\%$ of such pixels containing fluxes higher than the peak of the histogram. The slope of this line is -0.86 . We extrapolate the linear fit toward fainter fluxes to the point where all the pixels in the image are accounted for (red dashed line). The red hashed area shows the missing flux component corresponding to $1.9 \text{ nW m}^{-2} \text{ sr}^{-1}$ in the K_s -band.

galaxies.

3.2. The Stellar Component of NIR Light

The integrated intensity from stars in the NIR (at Earth) is comparable to that of resolved galaxies (as determined by models, such as those of Levenson et al. 2007, or by integrated star counts, as discussed below). Thus, in terms of measuring the IGL, it is crucial to be able to separate stars from galaxies accurately. In K10 we demonstrate that we are robustly separating stars from galaxies in our analysis. Thus, we are able to derive the stellar contribution to total NIR light with star counts from $15 < JHK_s < 24$, while groups making unresolved measurements of the total NIR EBL must assume stellar distribution models to remove the NIR light due to stars from their measurements. The integrated starlight from our star counts is $14.7 \pm 2.4 \text{ nW m}^{-2} \text{ sr}^{-1}$ in J -band, $10.1 \pm 1.9 \text{ nW m}^{-2} \text{ sr}^{-1}$ in H -band, and $7.6 \pm 1.8 \text{ nW m}^{-2} \text{ sr}^{-1}$ in K_s -band.

Four of our five fields are at Galactic latitudes of $b \sim 50$, and one is at $b \sim 70$ (we average over all five in the numbers quoted above). Looking at the modeled starlight as a function of Galactic latitude in Levenson et al. (2007), we find the average NIR light due to stars in their models at these latitudes is $\sim 7 \text{ nW m}^{-2} \text{ sr}^{-1}$ in K -band and $\sim 16 \text{ nW m}^{-2} \text{ sr}^{-1}$ in J -band, in good agreement with our measured values. Thus, it appears that recent total NIR EBL measurements are removing the stellar component correctly. However, as pointed out in K10, cool dwarf stars may contaminate the galaxy counts fainter than $JHK \sim 19$, suggesting that perhaps both IGL measurements and direct total NIR EBL measurements retain some level of stellar contamination, but this would not affect any discrepancy between the two. TeV γ -ray observations are concerned with the NIR background along the entire path length to

the blazars and are unaffected by Galactic NIR starlight due to its local origin.

4. COMPARISON WITH PREVIOUS RESULTS

In Figure 5 we show our IGL results alongside a summary of measurements of the NIR IGL (black symbols) and EBL (red symbols) over the past decade, including results obtained via integrated galaxy counts (Madau & Pozzetti 2000; Totani et al. 2001; Thompson 2003), via total light minus stars and zodiacal light (Dwek & Arendt 1998; Hauser et al. 1998; Gorjian et al. 2000; Wright 2001; Cambr sy et al. 2001; Matsumoto et al. 2005; Levenson et al. 2007), and via TeV γ -ray opacity (blue hashed area) (Aharonian et al. 2006).

The blue hashed area of Figure 5 shows the allowed (1σ) NIR EBL intensity ($14 \pm 4 \text{ nW m}^{-2} \text{ sr}^{-1}$) derived from High Energy Stereoscopic System (HESS) observations of TeV blazars (Aharonian et al. 2006). Mazin & Raue (2007) use 13 TeV blazars and a grid of NIR background intensities to further constrain the NIR EBL and find approximate agreement with the results of Aharonian et al. (2006). As noted earlier, however, estimates of the NIR EBL from TeV γ -ray opacity measurements rely on assumptions about the intrinsic SEDs of blazars and that of the EBL, both of which are poorly constrained observationally. Our results (black diamonds) are some 10–20% higher than previous estimates of the IGL, which puts them closer to EBL estimates from TeV blazar observations and the most recent total NIR EBL measurements.

A large NIRBE has been found by several groups, with perhaps the most striking result being that of Matsumoto et al. (2005). This excess, when combined with other NIR and optical background measurements, showed an apparent spectral break around $1 \mu\text{m}$. The excess was originally attributed to PopIII stars, with the break corresponding to the redshifted Lyman limit for these stars at $z \sim 10$. However, a search for the possible absorption imprint of this break on the γ -ray SED of blazars did not find evidence for such a feature (Dwek et al. 2005).

Madau & Silk (2005) discuss the implications of a NIRBE due to massive PopIII stars in the early universe and demonstrate that an excess of even a few $\text{nW m}^{-2} \text{ sr}^{-1}$ in the J -band would imply energetic requirements that are “uncomfortably high”. They note that $\sim 5\%$ of baryons would be formed into such stars by a redshift of 9 (roughly twice the fraction converted into stars since then) and that the metals created in these PopIII stars would have to be hidden in intermediate mass black holes (IMBHs) for the universe to avoid exceeding solar metallicity by redshift of 9. They point out that the IMBHs themselves could produce the NIR excess as miniquasars, as suggested by Santos et al. (2002), but that accretion onto these IMBHs would dominate the soft X-ray background and their mass density in the present day universe would exceed that of black holes found in galactic nuclei by 3 orders of magnitude. Finally, they show that the ionizing flux produced by these PopIII stars would exceed by 3 orders of magnitude that required to produce the WMAP observed electron scattering depth at $z = 17$.

TABLE 2
NIR INTEGRATED GALAXY LIGHT (νI_ν ; $\text{nW m}^{-2} \text{sr}^{-1}$)

	J^a	H	K_s^b
This work ^c	11.7 (+3) \pm 2.6	11.5 (+3) \pm 1.5	10.0 (+1.9) \pm 0.8
Madau & Pozzetti (2000)	9.7 ^{+3.0} _{-1.9}	9.0 ^{+2.6} _{-1.7}	7.9 ^{+2.0} _{-1.2}
Totani et al. (2001)	10.9 \pm 1.1	N/A	8.3 \pm 0.8
Thompson (2003) ^d	N/A	7.0	N/A

^a Madau & Pozzetti (2000) J -band is centered at $1.1\mu\text{m}$ while this and other studies listed are centered at $1.25\mu\text{m}$.

^b This work is done at $K_s(2.12\mu\text{m})$ while Madau & Pozzetti (2000) and Totani et al. (2001) are at $K(2.2\mu\text{m})$.

^c Missing flux estimates are given in parentheses next to our measured values for the IGL. The missing flux in the J and H -bands are taken from Thompson et al. (2007) and for K_s -band the value is derived as described in Section 3.1. The confidence intervals given are the 1σ error estimates from the galaxy counts fits described in Section 3.

^d Lower limit.

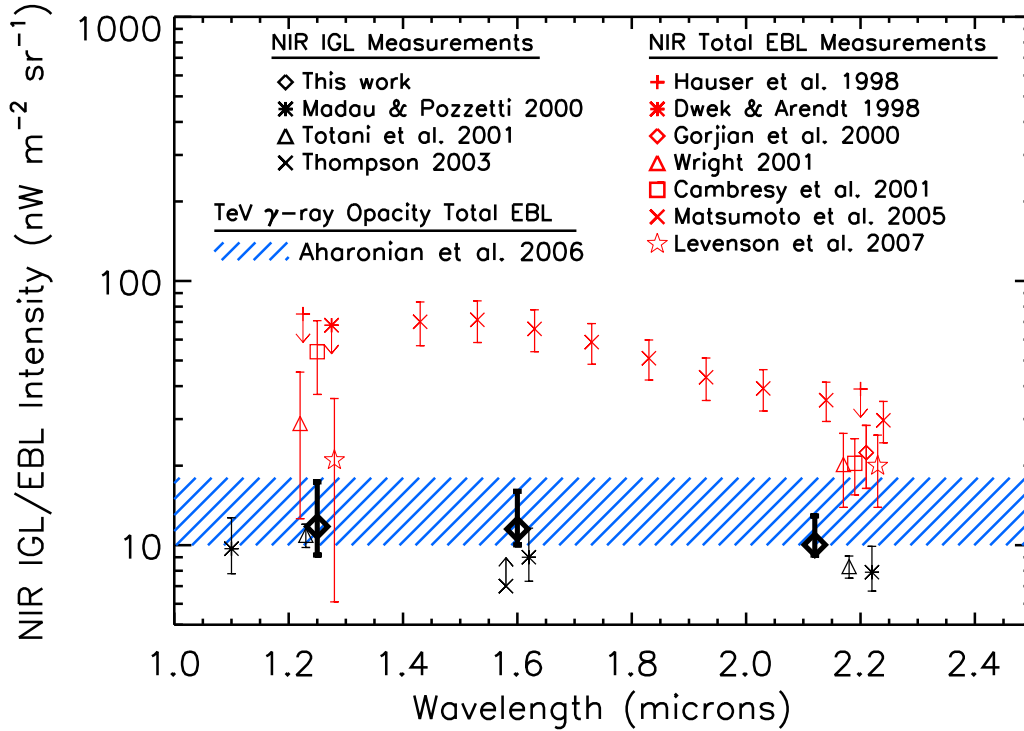


FIG. 5.— NIR IGL and EBL measurements over the past decade as a function of wavelength (μm). This work (black diamonds) and a summary of measurements of the NIR IGL (other black symbols) via integrated galaxy counts (Madau & Pozzetti 2000; Totani et al. 2001; Thompson 2003), total EBL (red symbols) via total light minus stars and zodiacal light (Dwek & Arendt 1998; Hauser et al. 1998; Gorjian et al. 2000; Wright 2001; Cambresy et al. 2001; Matsumoto et al. 2005; Levenson et al. 2007), and via TeV γ -ray opacity measurements (blue hashed area) (Aharonian et al. 2006). The range indicated for the γ -ray work shows the 1σ error range. Note that data points at $1.25, 1.6$, and $2.2\mu\text{m}$ have been shifted slightly in their abscissa values for clarity. Arrows are used to denote upper and lower limits and otherwise error bars represent 1σ confidence levels. Our results bring the measurement of the IGL into better agreement with TeV γ -ray observations and the most recent total total NIR EBL measurements. The lower limits on our data points show the 1σ error estimates associated with the galaxy counts integration described in Section 3, while the upper limits show these same 1σ error estimates plus the missing flux component derived in Section 3.1 and shown in Table 2

5. SUMMARY

We have presented measurements of the IGL in J , H , and K_s using deep wide-field NIR photometry in combination with ultra-deep MOIRCS K_s -band data and selections from the literature. These results place the best current constraints on the total NIR light from resolved galaxies and serve as a new lower limit to the total NIR EBL. While these results are in relative agreement with previous measurements, our numbers are 10 – 20% higher, bringing them into better agreement with those derived from γ -ray experiments and the most recent measurements of the total NIR EBL.

We find the IGL to be roughly isotropic, consistent with the expectation of large-scale isotropy in the EBL. We confirm that the starlight subtraction for the most recent total NIR EBL measurements is correct, so if there still exists a foreground subtraction issue in these measurements, it most likely is associated with the zodiacal light.

While our measurements cannot rule out the existence of a NIRBE due to PopIII stars or other exotic early universe objects, our new lower limits on the IGL and the upper limits found from TeV γ -ray experiments (Aharonian et al. 2006) could now be considered in rough agreement with the most recent total NIR EBL measurements in the J -band, and in near agreement in the K -band.

We thank the anonymous referee for their careful review of this article and their comments and suggestions that helped to improve the content and presentation of

this work.

We gratefully acknowledge support from the NSF grants AST 0708793 (A. J. B.) and AST 0709356 (L. L. C.), the University of Wisconsin Research Committee with funds granted by the Wisconsin Alumni Research Foundation, and the David and Lucile Packard Foundation (A. J. B.). R. C. K. was supported by a Wisconsin Space Grant Consortium Graduate Fellowship, a Sigma Xi Grant in Aid of Research and an NSF East Asia and Pacific Summer Institutes Fellowship during portions of this work.

This publication makes use of data products from the Two Micron All Sky Survey (2MASS), which is a joint project of the University of Massachusetts and the Infrared Processing and Analysis Center/California Institute of Technology, funded by the National Aeronautics and Space Administration and the National Science Foundation.

This work is based in part on data products from the UKIRT Infrared Deep Sky Survey (UKIDSS).

This work is based in part on observations obtained with WIRCcam, a joint project of CFHT, Taiwan, Korea, Canada, France, and the Canada-France-Hawaii Telescope (CFHT) which is operated by the National Research Council (NRC) of Canada, the Institut National des Sciences de l'Univers of the Centre National de la Recherche Scientifique of France, and the University of Hawaii.

This work is based in part on data collected at the Subaru Telescope, which is operated by the National Astronomical Observatory of Japan.

This work has made use of NASA's Astrophysics Data System.

REFERENCES

- Aharonian, F., Akhperjanian, A. G., Bazer-Bachi, A. R., Beilicke, M., Benbow, W., Berge, D., Bernlöhr, K., Boisson, C., Bolz, O., Borrel, V., Braun, I., Breitling, F., Brown, A. M., Chadwick, P. M., Chounet, L.-M., Cornils, R., Costamante, L., Degrange, B., Dickinson, H. J., Djannati-Ataï, A., Drury, L. O., Dubus, G., Emmanoulopoulos, D., Espigat, P., Feinstein, F., Fontaine, G., Fuchs, Y., Funk, S., Gallant, Y. A., Giebels, B., Gillesen, S., Glicenstein, J. F., Goret, P., Hadjichristidis, C., Hauser, D., Hauser, M., Heinzlmann, G., Henri, G., Hermann, G., Hinton, J. A., Hofmann, W., Holleran, M., Horns, D., Jacholkowska, A., de Jager, O. C., Khélifi, B., Klages, S., Komin, N., Konopelko, A., Latham, I. J., Le Gallou, R., Lemièrre, A., Lemoine-Goumard, M., Leroy, N., Lohse, T., Martin, J. M., Martineau-Huynh, O., Marcowith, A., Masterson, C., McComb, T. J. L., de Naurois, M., Nolan, S. J., Noutsos, A., Orford, K. J., Osborne, J. L., Ouchrif, M., Panter, M., Pelletier, G., Pita, S., Pühlhofer, G., Punch, M., Raubenheimer, B. C., Raue, M., Raux, J., Rayner, S. M., Reimer, A., Reimer, O., Ripken, J., Rob, L., Rolland, L., Rowell, G., Sahakian, V., Saugé, L., Schlenker, S., Schlickeiser, R., Schuster, C., Schwanke, U., Siewert, M., Sol, H., Spangler, R., Steenkamp, R., Stegmann, C., Tavernet, J.-P., Terrier, R., Théoret, C. G., Tluczykont, M., van Eldik, C., Vasileiadis, G., Venter, C., Vincent, P., Völk, H. J., & Wagner, S. J. 2006, *Nature*, 440, 1018
- Alexander, D. M., Bauer, F. E., Brandt, W. N., Schneider, D. P., Hornschemeier, A. E., Vignali, C., Barger, A. J., Broos, P. S., Cowie, L. L., Garmire, G. P., Townsley, L. K., Bautz, M. W., Chartas, G., & Sargent, W. L. W. 2003, *AJ*, 126, 539
- Barger, A. J., Cowie, L. L., & Wang, W. H. 2008, *ApJ*, 689, 687
- Bertin, E., & Arnouts, S. 1996, *A&AS*, 117, 393
- Brandt, W. N., Alexander, D. M., Hornschemeier, A. E., Garmire, G. P., Schneider, D. P., Barger, A. J., Bauer, F. E., Broos, P. S., Cowie, L. L., Townsley, L. K., Burrows, D. N., Chartas, G., Feigelson, E. D., Griffiths, R. E., Nousek, J. A., & Sargent, W. L. W. 2001, *AJ*, 122, 2810
- Cambresy, L., Reach, W. T., Beichman, C. A., & Jarrett, T. H. 2001, *ApJ*, 555, 563
- Dwek, E., & Arendt, R. G. 1998, *ApJ*, 508, L9
- Dwek, E., Krennrich, F., & Arendt, R. G. 2005, *ApJ*, 634, 155
- Giavalisco, M., Ferguson, H. C., Koekemoer, A. M., Dickinson, M., Alexander, D. M., Bauer, F. E., Bergeron, J., Biagetti, C., Brandt, W. N., Casertano, S., Cesarsky, C., Chatzichristou, E., Conselice, C., Cristiani, S., Da Costa, L., Dahlen, T., de Mello, D., Eisenhardt, P., Erben, T., Fall, S. M., Fasnacht, C., Fosbury, R., Fruchter, A., Gardner, J. P., Grogin, N., Hook, R. N., Hornschemeier, A. E., Idzi, R., Jogle, S., Kretchmer, C., Laidler, V., Lee, K. S., Livio, M., Lucas, R., Madau, P., Mobasher, B., Moustakas, L. A., Nonino, M., Padovani, P., Papovich, C., Park, Y., Ravindranath, S., Renzini, A., Richardson, M., Riess, A., Rosati, P., Schirmer, M., Schreier, E., Somerville, R. S., Spinrad, H., Stern, D., Stiavelli, M., Ströger, L., Urry, C. M., Vandame, B., Williams, R., & Wolf, C. 2004, *ApJ*, 600, L93
- Gorjian, V., Wright, E. L., & Chary, R. R. 2000, *ApJ*, 536, 550
- Hauser, M. G., Arendt, R. G., Kelsall, T., Dwek, E., Odegard, N., Weiland, J. L., Freudenreich, H. T., Reach, W. T., Silverberg, R. F., Moseley, S. H., Pei, Y. C., Lubin, P., Mather, J. C., Shafer, R. A., Smoot, G. F., Weiss, R., Wilkinson, D. T., & Wright, E. L. 1998, *ApJ*, 508, 25
- Hauser, M. G., & Dwek, E. 2001, *ARA&A*, 39, 249
- Kajisawa, M., Konishi, M., Suzuki, R., Tokoku, C., Uchimoto, Y. K. Y. T., Akiyama, M., Ichikawa, T., Ouchi, M., Omata, K., Tanaka, I., Nishimura, T., & Yamada, T. 2006, *PASJ*, 58, 951
- Kashlinsky, A. 2005, *Phys. Rep.*, 409, 361

- Keenan, R. C., Trouille, L., Barger, A. J., Cowie, L. L., & Wang, W. H. 2010, *ApJS*, 186, 94
- Kron, R. G. 1980, *ApJS*, 43, 305
- Lawrence, A., Warren, S. J., Almaini, O., Edge, A. C., Hambly, N. C., Jameson, R. F., Lucas, P., Casali, M., Adamson, A., Dye, S., Emerson, J. P., Foucaud, S., Hewett, P., Hirst, P., Hodgkin, S. T., Irwin, M. J., Lodieu, N., McMahon, R. G., Simpson, C., Smail, I., Mortlock, D., & Folger, M. 2007, *MNRAS*, 379, 1599
- Levenson, L. R., Wright, E. L., & Johnson, B. D. 2007, *ApJ*, 666, 34
- Lilly, S. J., Cowie, L. L., & Gardner, J. P. 1991, *ApJ*, 369, 79
- Lockman, F. J., Jahoda, K., & McCammon, D. 1986, *ApJ*, 302, 432
- Madau, P., & Pozzetti, L. 2000, *MNRAS*, 312, L9
- Madau, P., & Silk, J. 2005, *MNRAS*, 359, L37
- Maihara, T., Iwamuro, F., Tanabe, H., Taguchi, T., Hata, R., Oya, S., Kashikawa, N., Iye, M., Miyazaki, S., Karoji, H., Yoshida, M., Totani, T., Yoshii, Y., Okamura, S., Shimasaku, K., Saito, Y., Ando, H., Goto, M., Hayashi, M., Kaifu, N., Kobayashi, N., Kosugi, G., Motohara, K., Nishimura, T., Noumaru, J., Ogasawara, R., Sasaki, T., Sekiguchi, K., Takata, T., Terada, H., Yamashita, T., Usuda, T., & Tokunaga, A. T. 2001, *PASJ*, 53, 25
- Matsumoto, T. 2001, in *IAU Symposium*, Vol. 204, *The Extragalactic Infrared Background and its Cosmological Implications*, ed. M. Harwit & M. G. Hauser, 87
- Matsumoto, T., Matsuura, S., Murakami, H., Tanaka, M., Freund, M., Lim, M., Cohen, M., Kawada, M., & Noda, M. 2005, *ApJ*, 626, 31
- Mazin, D., & Raue, M. 2007, *A&A*, 471, 439
- Minowa, Y., Kobayashi, N., Yoshii, Y., Totani, T., Maihara, T., Iwamuro, F., Takami, H., Takato, N., Hayano, Y., Terada, H., Oya, S., Iye, M., & Tokunaga, A. T. 2005, *ApJ*, 629, 29
- Santos, M. R., Bromm, V., & Kamionkowski, M. 2002, *MNRAS*, 336, 1082
- Skrutskie, M. F., Cutri, R. M., Stiening, R., Weinberg, M. D., Schneider, S., Carpenter, J. M., Beichman, C., Capps, R., Chester, T., Elias, J., Huchra, J., Liebert, J., Lonsdale, C., Monet, D. G., Price, S., Seitzer, P., Jarrett, T., Kirkpatrick, J. D., Gizis, J. E., Howard, E., Evans, T., Fowler, J., Fullmer, L., Hurt, R., Light, R., Kopan, E. L., Marsh, K. A., McCallon, H. L., Tam, R., Van Dyk, S., & Wheelock, S. 2006, *AJ*, 131, 1163
- Steffen, A. T., Barger, A. J., Capak, P., Cowie, L. L., Mushotzky, R. F., & Yang, Y. 2004, *AJ*, 128, 1483
- Thompson, R. I. 2003, *ApJ*, 596, 748
- Thompson, R. I., Eisenstein, D., Fan, X., Rieke, M., & Kennicutt, R. C. 2007, *ApJ*, 657, 669
- Totani, T., Yoshii, Y., Iwamuro, F., Maihara, T., & Motohara, K. 2001, *ApJ*, 550, L137
- Trouille, L., Barger, A. J., Cowie, L. L., Yang, Y., & Mushotzky, R. F. 2008, *ApJS*, 179, 1
- . 2009, *ApJ*, 703, 2160
- Wang, W. H., Barger, A. J., & Cowie, L. L. 2009, *ApJ*, 690, 319
- Wright, E. L. 2001, *ApJ*, 553, 538
- Yang, Y., Mushotzky, R. F., Steffen, A. T., Barger, A. J., & Cowie, L. L. 2004, *AJ*, 128, 1501